Received: 31 March 2018 | Revised: 13 June 2018 | Accepted: 26 June 2018

DOI: 10.1002/bit.26783

ARTICLE

WILEY BIOTECHNOLOGY BIOENGINEERING

Outline-etching image segmentation reveals enhanced cell chirality through intercellular alignment

Yaozhun Huang[1] | Yuanye Bao[1] | Hoi Kwan Kwong[1] | Ting-Hsuan Chen[1] | Miu Ling Lam[2]

[1]Department of Mechanical and Biomedical Engineering, City University of Hong Kong, Kowloon, Hong Kong

[2]School of Creative Media, City University of Hong Kong, Kowloon, Hong Kong

Correspondence
Ting-Hsuan Chen, Department of Mechanical and Biomedical Engineering, City University of Hong Kong, P6415, Yeung Kin Man Academic Building, 83 Tat Chee Avenue, Kowloon, Hong Kong Administrative Region.
Email: thchen@cityu.edu.hk
Miu Ling Lam, School of Creative Media, City University of Hong Kong, M7090, Run Run Shaw Creative Media Centre, 18 Tat Hong Avenue, Kowloon, Hong Kong Administrative Region.
Email: miu.lam@cityu.edu.hk

Funding information
National Natural Science Foundation of China, Grant/Award Number: 61502406; Science Technology and Innovation Committee of Shenzhen Municipality, Grant/Award Number: JCYJ20170307091338607; Research Grants Council, University Grants Committee, Grant/Award Numbers: 21214815, 11217217, 11277516; Croucher Foundation, Grant/Award Number: 9500016

Abstract

Cells cultured on micropatterns exhibit a chiral orientation, which may underlie the development of left–right asymmetry in tissue microarchitectures. To investigate this phenomenon, fluorescence staining of nuclei has been used to reveal such orientation. However, for images with high cell density, analysis is difficult because of the overlapping nuclei. Here, we report an image processing method that can acquire cell orientations within dense cell populations. After initial separation based on Boolean addition of binarized images using global and adaptive thresholds, the overlapping nucleus contours in the binarized images were segmented by iteratively etching the outlines of nuclei, which allowed the orientations of each cell to be extracted from densely packed cell clusters. In applying this technique to cultured C2C12 myoblasts in micropatterned stripes on different substrates, we found an enhanced chiral orientation on glass substrate. More important, this enhanced chirality was consistently observed with increased intercellular alignment and independent of cell–cell distance or cell density, suggesting that intercellular alignment plays a role in determining the chiral orientation. By segmenting single cells with intact orientation, this technique offers an automated method for quantitative analysis with improved accuracy, providing an essential tool for studying left–right asymmetry and other morphogenic dynamics in tissue formation.

KEYWORDS
cell chirality, cell orientation, image segmentation, morphogenesis

1 | INTRODUCTION

Differences in cell orientation are commonly observed in many tissue microarchitectures, including the myocardium (Streeter, Spotnitz, Patel, Ross, & Sonnenblick, 1969), vasculature (Chiu, Chen, Chen, Lee, & Lee, 2004), and connective tissue (Vunjak-Novakovic, Altman, Horan, & Kaplan, 2004). These geometric features are considered to be essential in tissue and organ functioning. For example, contractility of muscular tissue requires specific layer-by-layer orientations with different angles (Streeter et al., 1969). In cardiac tissue, cell orientation guides the anisotropic propagation of action potential (Kim et al., 2010), which regulates electrophysiological signals and triggers mechanical actions. An understanding of cell orientation is thus of vital importance.

Emerging evidence suggests that cells may exhibit a chirality when cultured on a micropatterned substrate (Chen, Hsu, et al., 2012; Wan et al., 2011). We previously reported that vascular mesenchymal cells can orient at a specific chiral angle relative to the micropattern boundaries. This intrinsic chirality can subsequently be amplified, leading to a coherent chiral orientation throughout the rest of the culture. Moreover, accompanying cell assembly, the chiral orientation later

causes the formation of a tissue-like structure with a specific, left–right biased pattern (Chen, Hsu, et al., 2012; Chen, Zhu, et al., 2012). Importantly, the chiral orientation is not only observed in vascular mesenchymal cells but in other cell types (Zhu, Kwong, Bao, & Chen, 2017). As the formation of coherent cell orientation is driven by autocatalytic feedback based on intercellular alignment (Junkin, Leung, Whitman, Gregorio, & Wong, 2011), it is believed that intercellular alignment may play a role in amplifying the cell chirality. However, direct evidence to support this hypothesis has been lacking.

In conventional approaches, fluorescence-stained nuclei are used to reveal cellular orientation (Raymond, Ray, Kaur, Singh, & Wan, 2016), and a global threshold is commonly used to binarize the images for further analysis. Unfortunately, in a culture with high cell density, densely packed cell cluster makes the contours of nuclei overlapping. As a result, after image binarization, a cell cluster in a binary image may be recognized as one bright region containing multiple cells, which makes the orientation analysis inaccurate. Many methods have been proposed to address this issue. Watershed methods (Beucher & Lantuejoul, 1979; Cheng & Rajapakse, 2009; Meyer, 1994) have been widely used in cell segmentation. The main drawback of the watershed approach is oversegmentation and further processing is often needed. In recent years, machine learning has become increasingly popular in cell segmentation and analysis (Litjens et al., 2017; Ronneberger, Fischer, & Brox, 2015), but the lack of training data, annotations, and labelled images remain the key challenges.

Here we report an image processing method that can segment densely packed cell clusters into individual cells without mistaking the orientation information. Boolean addition of binarized images using global and adaptive thresholds was first used for initial segmentation. To further segment the clusters into single cells, we applied an algorithm we named the "outline-etching method," which iteratively etches the outline of bright regions, enabling the segmentation of single nuclei from a cluster without affecting the cell orientation. We applied this method to study the culture of C2C12 myoblasts, with a focus on the dependence of cell chirality on the substrate material, cell density, and intercellular alignment. With the advantages of simple implementation and accurate analysis, our method provides a new approach for analyzing the development of cell chirality, with implications for assessing cell–cell communication in tissue morphogenesis and regeneration.

2 | MATERIALS AND METHODS

2.1 | Cell culture and fluorescence imaging

C2C12 mouse myoblasts (American Type Culture Collection, Manassas, VA) were cultured in Dulbecco's modified Eagle's medium (4 mM L-glutamine, 4,500 mg/L glucose, 1 mM sodium pyruvate, and 1.5 g/L sodium bicarbonate; Life Technologies, Carlsbad, CA), supplemented with 10% fetal bovine serum and 1% penicillin–streptomycin (Life Technologies, Carlsbad, CA). The cells were passaged at a density of 2,200 cells/cm^2 every 2 days, with passage number P8–P12 used in the experiment. For experiments on micropatterns, cells were seeded on cell-adherent stripes with a density of 75,000 cells/cm^2 for 30 min and kept at 37°C in a humidified incubator (5% CO_2 and 95% air) for 12 hr. To stain the nuclei, the cells were rinsed with Dulbecco's phosphate buffered saline, followed by application of 4% paraformaldehyde for 15 min, 0.1% Triton X-100 for 10 min, and 4,6 diamidino-2 phenylindone (300 nM, Thermo Fisher Scientific, Waltham, MA) staining for 5 min. Fluorescence images were then acquired using an inverted fluorescence microscope (Nikon, Minato, Tokyo, Japan).

2.2 | Microfabrication

Micropatterns were fabricated on glass or polydimethylsiloxane (PDMS) substrate using a photolithography process. For the glass substrate, a glass slide was cleaned with piranha solution (H_2SO_4: H_2O_2 = 3:1). For the PDMS substrate, PDMS was spread on cleaned glass, with overnight baking at 70°C for curing, followed by 2 min plasma treatment (800 mTorr, 30 W). Next, both substrates were coated with hexamethyldisilazane (HMDS; Sigma-Aldrich, St. Louis, MO; 5 min by vapor deposition), followed by spin-coating with 1.4 μm AZ5214 photoresist (PR; AZ Electronic Materials, Luxembourg). UV exposure and development (AZ400K; AZ Electronic Materials, Luxembourg) was conducted to obtain micropatterned stripes (PR removed, 1 cm × 200 μm). The substrate was then treated with 2 min plasma (800 mTorr, 30 W) and another HMDS coating (5 min by vapor deposition). After coating with fibronectin solution (20 μg/ml; Life Technologies, Carlsbad, CA), the chip was washed with absolute ethanol on an orbital shaker to remove the remaining PR. Before cell seeding, the chip was incubated in 1–2% pluronic F127 (Sigma-Aldrich, St. Louis, MO) in deionized water for 50 min to cover the exposed HMDS regions, creating cell-repellent surfaces.

2.3 | Image binarization

The image analysis is summarized in Figure 1 (MATLAB source code available in the Supporting Information). First, the gray-scale raw image obtained from the fluorescence microscopy (Step 1 in Figure 1) was adjusted as follows: after rescaling to 8-bit and application of a Gaussian filter to reduce intensity variation and noise, the image was binarized with a global threshold value obtained by Otsu's method (Otsu, 1979), which classifies foreground and background pixels by minimizing intra-class variance while maximizing interclass variance. After iterative calculation by a discriminant criterion, the optimal threshold was then used to binarize the foreground and background pixels to 1 (white) and 0 (black), respectively (Step 2 in Figure 1).

2.4 | Cluster identification

After the initial binarization, the processed image contained bright regions of single cells and cell clusters (Step 2 in Figure 1). The orientation of single cells can be determined based on the shapes of these regions. However, the contours of nuclei in cell clusters overlap, so additional image segmentation is necessary to determine the orientation of each cell in a cluster. To distinguish between single cells and cell

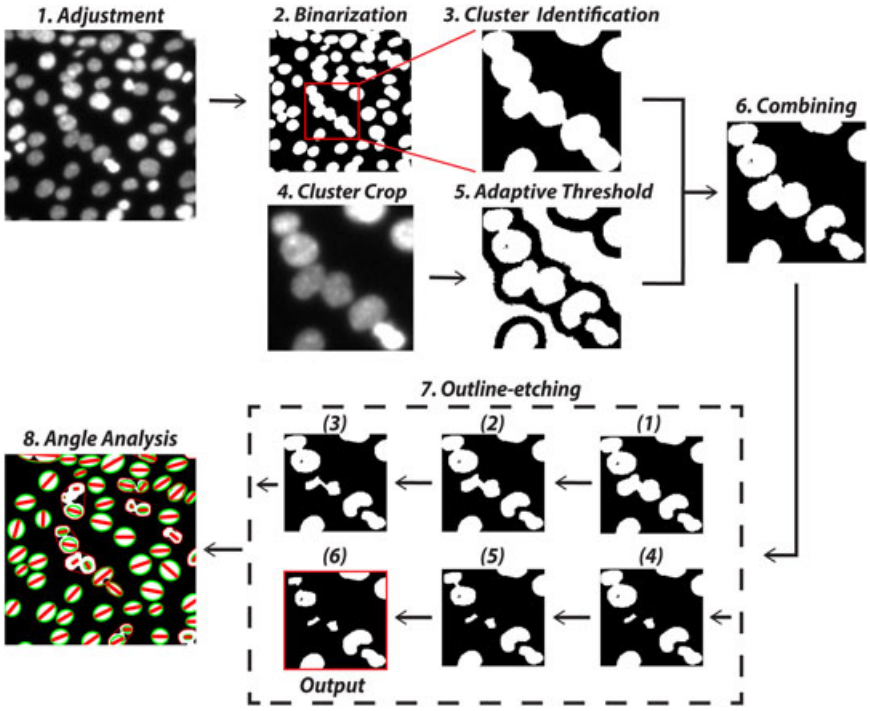

FIGURE 1 Flow chart of image analysis pipeline. The original fluorescence image was first adjusted, followed by Boolean addition of binarized images using global and adaptive threshold (upper half). The identified cluster was then processed using the "outline-etching" method to further segment single cells from a cluster for determination of cell orientations (lower half) [Color figure can be viewed at wileyonlinelibrary.com]

clusters, we introduced solidity, defined as the ratio between a region's area and the area of the minimum convex hull surrounding that region. For regions representing a single nucleus, the convex hulls tightly wrap around the cell regions, yielding a solidity value close to 1. For cell clusters consisting of concave regions at the cell connecting sites, the solidity value is lower. In our case, regions with solidity lower than 0.85 were identified as clusters (Step 3 in Figure 1).

2.5 | Adaptive thresholding

The positions of all identified clusters in the binary image (Step 3 in Figure 1) were used to crop the original gray-scale image (Step 4 in Figure 1). Next, an open process was applied to the subimages to remove small objects from the foreground. In brief, open process refers to a process of morphological erosion followed by dilation with a structuring element. As such, it enables morphological noise removal while keeping the cell region intact. After the open process, background noise is suppressed and the regions containing the nuclei are preserved.

Next, for the subimages after the open process (denoted as $\boldsymbol{I}_o$), adaptive thresholding was conducted. Different from the global threshold that is applied to all pixels, adaptive thresholding adjusts the threshold value locally to accommodate the uneven lighting conditions during image acquisition. Mathematically, adaptive thresholding assumes that smaller image regions are more likely to have approximately uniform illumination. Thus, an individual threshold for each pixel was assigned based on the range of intensity values in its neighborhood. The algorithm convolves the image patch $\boldsymbol{I}_o$ with a 25×25 averaging kernel $\boldsymbol{S}_o$ to obtain the mean of the local intensity distribution, as summarized below:

$$\boldsymbol{I}_c = \boldsymbol{I}_o(x, y) * \boldsymbol{S}_o(x, y) = \iint \boldsymbol{I}_o(x', y')\boldsymbol{S}_o(x-x', y-y')dx'dy', \quad (1)$$

Afterwards, the final processed image was calculated as $\boldsymbol{I}_{at} = \boldsymbol{I}_c - \boldsymbol{I}_o - 5$. As shown (Step 5 in Figure 1), in a cluster, the concavity between each nucleus was highlighted and the contour of clusters became clear. We then combined the information from both global and adaptive thresholding by a simple Boolean addition to merge the binary images of Steps 3 and 5 in Figure 1. A combined image was then obtained with enhanced concave regions (Step 6 in Figure 1) in which the cluster was broken down into individual nuclei and smaller clusters.

2.6 | Outline-etching

Following another open process to remove noise and small pieces, some single cells could be segregated from their original clusters. However, a number of clusters still needed further segmentation. After using the aforementioned solidity for identifying these remaining clusters, we then used an erosion-based iterative algorithm, named "outline-etching," to decompose the clusters into smaller regions with preserved orientation information of each cell (Step 7 in Figure 1). In each iteration in the outline-etching, the outermost layer of white pixels of a cluster was eroded. As a result, the cavities at the conjunction between cells expanded, leading to a cleavage between nuclei. Single cells segmented from the clusters with high solidity would then escape the next iteration, whereas clusters with lower solidity would proceed iteratively through the outline-etching process until all clusters were decomposed into single nuclei.

2.7 | Angle analysis

After image segmentation, the orientation of each identified nucleus was obtained based on the long axis of its surrounding ellipse (Step 8 in Figure 1). The orientation angle was defined as the acute angle θ between the long axis of the cell nucleus relative to the horizontally

aligned micropattern boundaries (Figure 2a,b). The angle θ is defined as positively oriented when the acute angle θ is within [0, 90] and negatively oriented when θ is within [−90, 0]. Thus, the percentages of positively and negatively aligned cells within one micropatterned stripe can be calculated. The chirality can then be determined by the significant difference between these two percentages collected from multiple stripes. To calculate cell density, we used total cell counts divided by the stripe area in the image. To study intercellular alignment, we used $|\Delta\theta|$, the absolute value of the acute angle difference between a chosen cell and its neighbors with cell–cell distance of less than 55 μm (120 pixels). Note that the range of cell–cell distances less than 55 μm include pairs of direct neighbors, pairs of indirect neighbors, and pairs of cells with many other cells between them. Next, the $|\Delta\theta|$ values of all of the cells were collected and averaged to plot a histogram against cell–cell distance.

2.8 | Analysis of cell–cell distance of direct neighbors

A Voronoi diagram was used to investigate the cell–cell distance between pairs of direct neighbors (Aurenhammer, 1991). After identifying individual nuclei, their centroids were taken as set points to build a Voronoi diagram, which partitions the two-dimensional plane into regions of convex polygons. Based on the distance between set points, perpendicular bisectors were inserted to comprise a corresponding convex polygon. For a selected nucleus, the cell–cell distances between direct neighbors were identified and calculated based on shared Voronoi vertices or edges within the Voronoi diagram.

2.9 | Statistical analysis

Student's t test was applied to compare the difference between the percentages of cells with negative and positive orientations. The confidence level was set to 0.05 for all statistical tests. Statistical significance was indicated by ns ($p > 0.05$), * ($p \le 0.05$), ** ($p \le 0.01$), *** ($p \le 0.001$), or **** ($p \le 0.0001$).

3 | RESULTS

3.1 | Accuracy of cell orientation determination

We first evaluated the improved accuracy resulting from the outline-etching method. To demonstrate the ability to segment

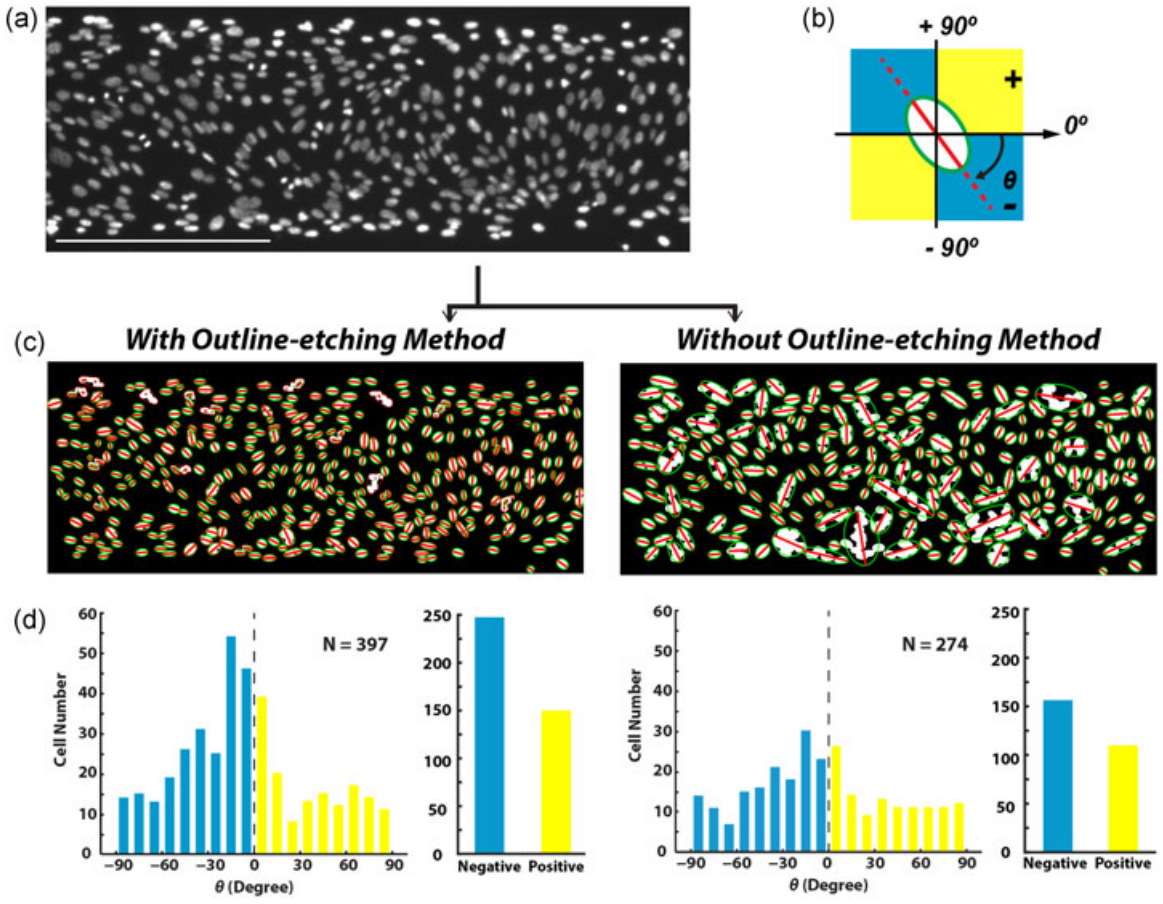

FIGURE 2 Accuracy of cell orientation determination improved by the outline-etching method. (a) The original fluorescence microscopic image with high cell density (scale bar: 300 μm). (b) The nucleus orientation θ defined by the acute angle between the long axis of the cell nucleus relative to the horizontally aligned micropattern boundary. (c) The obtained cell orientation from clusters with or without the outline-etching method. Red lines mark the long axis of the nucleus. (d) The histogram of cell orientation of (c) [Color figure can be viewed at wileyonlinelibrary.com]

cell nuclei with overlapping contours, we measured the cell orientation angles from an original fluorescence image with high cell density (Figure 2a,b). The result showed that, using the outline-etching method, large clusters can be successfully segmented into single nuclei with accurate cell orientations even when cells are very close (Figure 2c). In contrast, when only a global threshold was applied, some clusters were wrongly classified as single nuclei, which misrepresented the cell orientation (Figure 2c). In addition, the outline-etching method also increased the number of nuclei available for statistical analysis (from 274 to 397; Figure 2d). Thus, with effective segmentation, the cell orientation distribution can be revealed with improved cell number and accuracy, which allows the correct measurement of chirality in cell orientation (Figure 2d).

3.2 | Unchanged nucleus orientation after processing

To confirm that the outline-etching method can separate cell nuclei without affecting the orientation information, we compared the measured cell orientation with and without the outline-etching using an original fluorescence image with low cell density, in which the orientation of well-separated single cells without the outline-etching method served as the ground truth (Figure 3a,b). By collecting nucleus orientations after seven iterations of the outline-etching process, a comparison map was obtained (Figure 3c). The corresponding angles between these two sets (without/with outline-etching) regress as a line with a slope close to 1 (the regression equation is shown in Figure 3c). The R^2 is 0.9984, suggesting a very small variance between the data and the linear regression. Thus, the analysis confirmed that, while the size of the nucleus decreased, the orientation angle was unchanged when using the outline-etching method.

3.3 | Chiral orientation enhanced by intercellular alignment

We next applied this imaging technique to investigate the dependence of the chiral orientation of C2C12 myoblasts on the substrate material, cell density, and intercellular alignment. Previously we reported that cell chirality is enhanced on glass substrate but not on PDMS substrate (Zhu et al., 2017), as indicated by more cells oriented with negative angles (Figure 4). While we previously concluded that the difference in substrate rigidity is the primary reason for this finding, how substrate rigidity can enhance cell chirality remained unclear.

To explore this question, we applied the outline-etching method to analyze the experimental results. We first compared cell density on glass and PDMS substrates and found that the cell density was indeed slightly lower on PDMS substrate than that on glass substrate (Figure 5a), suggesting a possible involvement of cell density in the enhanced chirality. To clarify this point, we extracted images with high cell density (>180,000 cells/cm^2) and low cell density (<50,000 cells/cm^2) on both glass and PDMS substrates (Figure 5b). Interestingly, for images with high or low cell density, we found that the chirality was always enhanced on glass substrate, that is, more cells oriented negatively with statistical significance (Figure 5c). Thus, while cell density was slightly different on these two substrates, it does not seem to play a role in regulating the expression of cell chirality.

We next investigated the role of intercellular alignment. Autocatalytic cell–cell alignment has been shown to be important for myogenesis (Junkin et al., 2011). Similarly, local (Edelstein-Keshet & Ermentrout, 1990; Wang et al., 2015) and global (Wan et al., 2011) alignment have both been revealed in regular and conditional culture at the multicellular level. To study it, we analyzed the absolute value of acute angle difference $|\Delta\theta|$ between one cell and its neighbors at a cell–cell distance of less than 55 μm (120 pixels). Cells within this distance include pairs of direct neighbors, pairs of indirect neighbors, and pairs of cells that are separated by many other cells. After

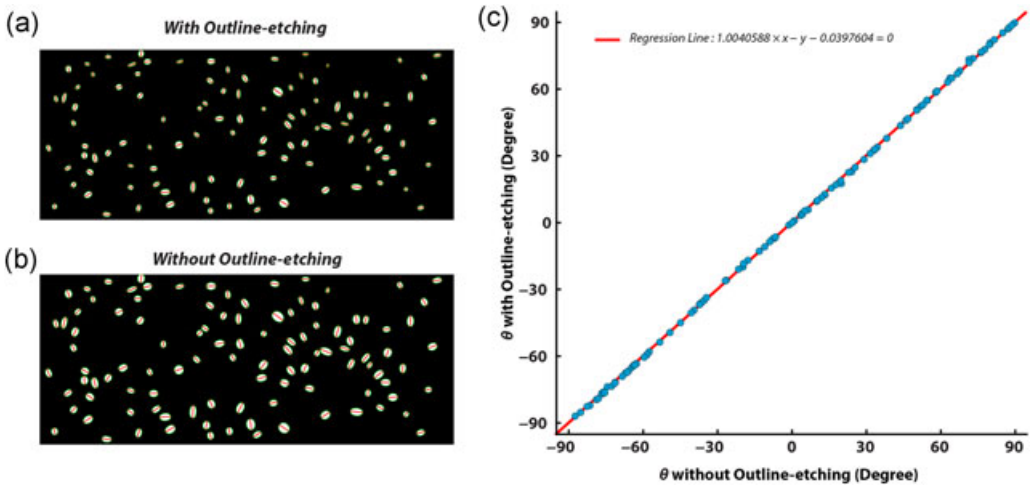

FIGURE 3 Unchanged nucleus orientation after using the outline-etching method. (a,b) Using an image with low cell density, the processed image with (a) or without (b) the outline-etching method. (c) Comparison of the cell orientations obtained from image analysis with and without the outline-etching method [Color figure can be viewed at wileyonlinelibrary.com]

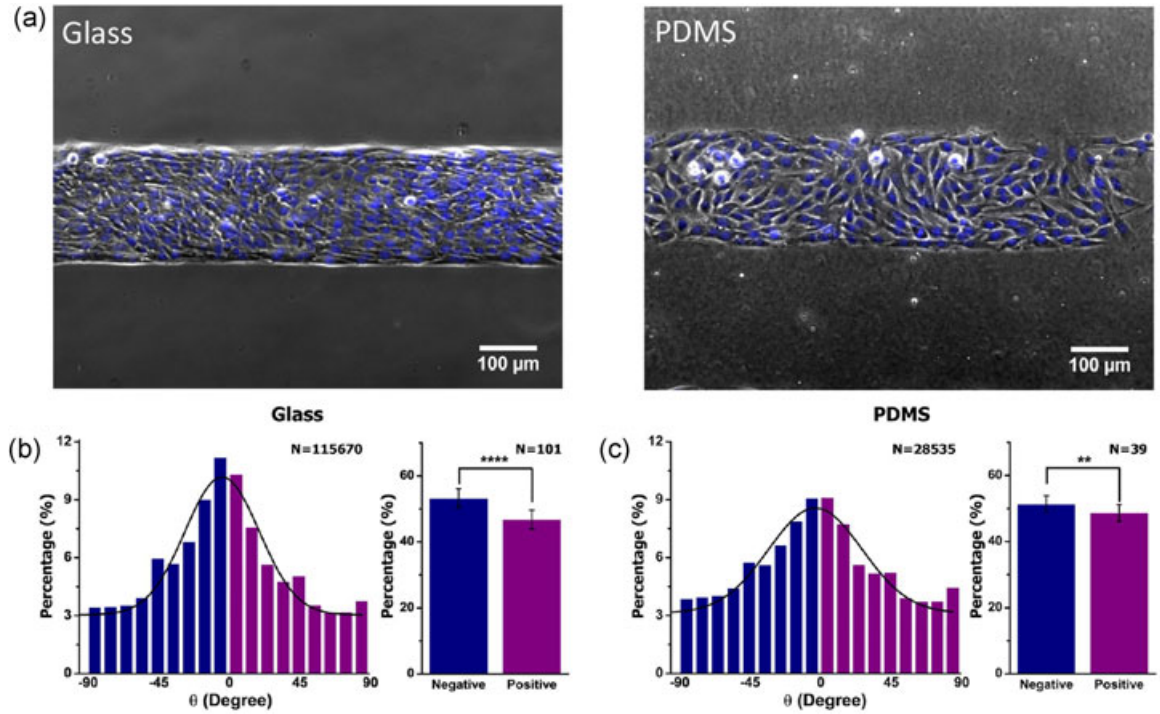

FIGURE 4 Chiral orientation of cells on different substrates. (a) Phase contrast microscopic images of cells in micropatterned stripes on glass or polydimethylsiloxane (PDMS) substrate. (b,c) Histogram of cell orientations on (b) glass and (c) PDMS substrates. The percentage of positively and negatively oriented cells in each stripe was averaged for multiple stripes, and the chirality was determined based on the statistically significant difference between these two percentages [Color figure can be viewed at wileyonlinelibrary.com]

collecting data from all of the cells and their neighbors, the $|\Delta\theta|$ values were averaged and plotted against the cell–cell distance. For images with low cell density (Figure 6a), we found that the $|\Delta\theta|$ was reduced with shorter cell–cell distance, indicating an improved intercellular alignment with a shorter cell–cell distance. Notably, the $|\Delta\theta|$ was always less for cells on glass substrate than for those on PDMS substrate. For images with high cell density, a decrease in $|\Delta\theta|$ was again observed with shorter cell–cell distance but $|\Delta\theta|$ reached a plateau when the cell–cell distance was greater than 20 μm (Figure 6b). Again, the $|\Delta\theta|$ was always less on glass substrate for the entire range of cell–cell distances, including the plateau value. Thus, the evenly reduced $|\Delta\theta|$ on glass substrate regardless of cell density suggests that improved intercellular alignment over a wide range of cell–cell distances could be the origin of enhanced chirality.

Interestingly, for the culture with high cell density, the $|\Delta\theta|$ reduced with short cell–cell distance but increased sharply towards a plateau when the cell–cell distance was greater than 20 μm (Figure 6b). As a comparison, in the culture with low cell density, we observed a gradual, smooth increase of $|\Delta\theta|$ with the increase of cell–cell distance, and no plateau was observed even when cell–cell distance reached 50 μm (Figure 6a). By analyzing the images using the Voronoi diagram (Figure 6c), we found that the average distance between direct neighbors decreased significantly with increasing cell density (Figure 6d). In particular, for images of cell densities higher than 180,000 cells/cm^2 and lower than 50,000 cells/cm^2, the average cell–cell distances of direct neighbors were 22–23 and 50 μm, respectively (Figure 6d). These distances between direct neighbors are consistent with the range of cell–cell distances with reduced $|\Delta\theta|$ before reaching the plateau (Figure 6a,b). Thus, the results suggest that the locally decreased $|\Delta\theta|$ before the plateau should be due to the local alignment between pairs of direct neighbors. More important, increased cell density does not seem to improve the intercellular alignment. Instead, it only reduces the distance between direct neighbors, leading to a shorter range of cell–cell distance with reduced $|\Delta\theta|$ before reaching the plateau. When cultured on glass substrate, other factors, such as substrate rigidity, can reduce the $|\Delta\theta|$ in a greater range of cell–cell distances, thereby improving the intercellular alignment with broader range and leading to an overall enhancement of chiral orientation.

4 | DISCUSSION AND CONCLUSIONS

In this study, we propose an outline-etching image segmentation for analyzing cell chirality (MATLAB source code available in the Supporting Information). We successfully extracted single cell's orientation from densely packed cell clusters with improved accuracy. As opposed to the use of conventional global thresholds, which is only suitable when there is clear background or foreground contrast over the entire image, the use of an adaptive threshold enables the analysis of fluorescence images with nonuniform illumination, providing the possibility to analyze the entire image without missing local information. Moreover, by implementing the outline-etching method, densely packed cell clusters can be successfully segmented into single cells without losing or mistaking the cell orientation. As such, our framework

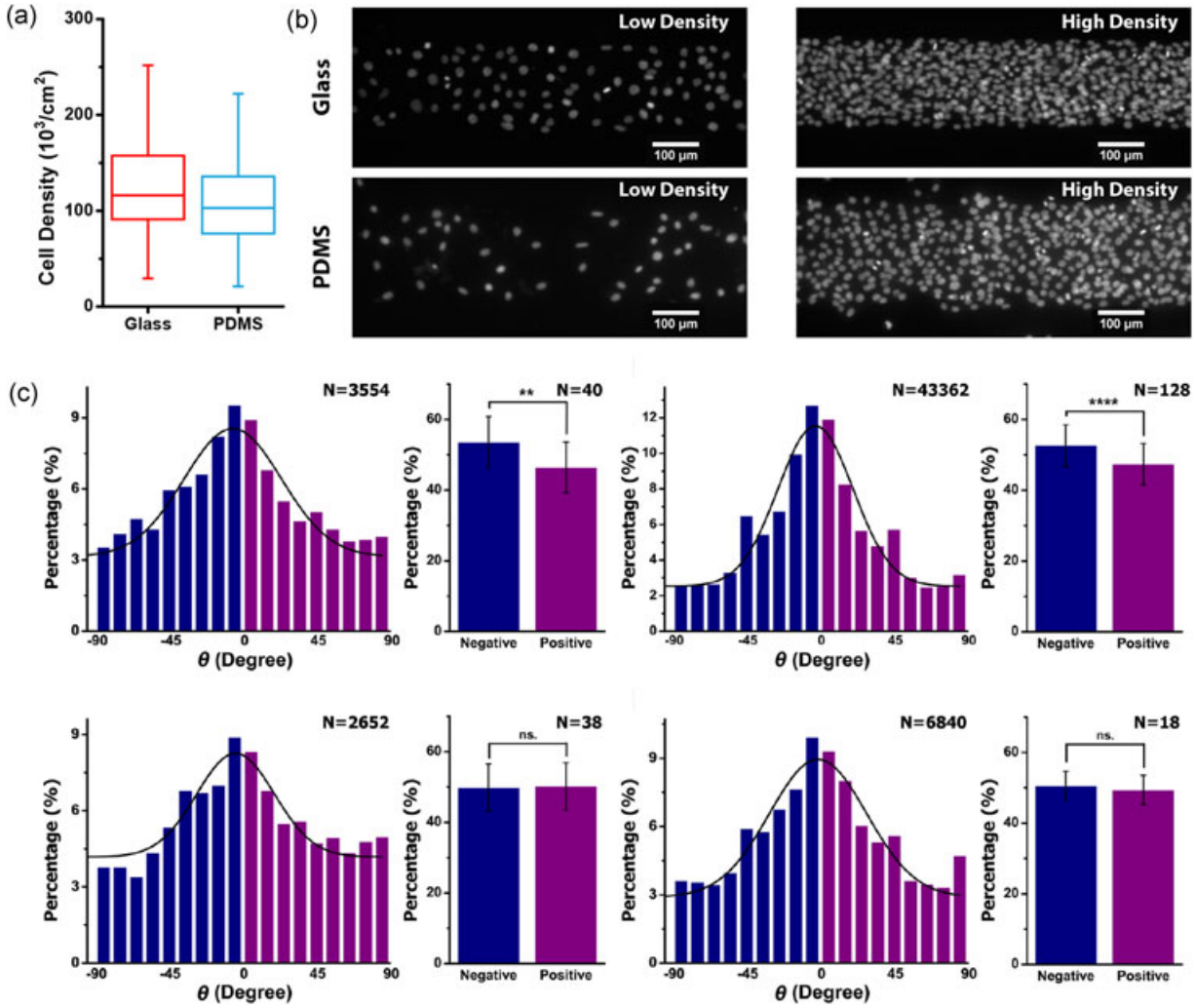

FIGURE 5 Chiral orientation of cells with different cell densities. (a) Cell density distribution within micropatterned stripes on glass and polydimethylsiloxane (PDMS) substrates. (b) Representative images of fluorescence-stained nuclei with high cell density (>180,000 cells/cm^2) and low cell density (<50,000 cells/cm^2) on glass and PDMS substrates. (c) Histogram of cell orientation on glass substrate with low cell density (upper-left), glass substrate with high cell density (upper-right), PDMS substrate with low cell density (lower-left), and PDMS substrate with high cell density (lower-right). The percentages of positively and negatively oriented cells in each stripe were averaged for multiple stripes, and the chirality was determined based on the statistically significant difference between these two percentages [Color figure can be viewed at wileyonlinelibrary.com]

is capable of improving accuracy and allowing the automatic generation of massive and enriched cellular information.

Note that the proposed outline-etching cell segmentation method is tailored for cell orientation analysis. For other applications of cell segmentation, it may not be suitable, as the bright region shrinks during the etching process. To solve this issue, it may be necessary to regrow the etched region or use a watershed approach to obtain the full cell area.

Based on the ability to isolate single cells from a dense cell population, our study of cell chirality revealed that intercellular alignment may underlie the enhancement of chiral orientation. Coherent chiral orientation has been reported previously (Chen, Hsu, et al., 2012), and cadherin-mediated cell–cell contact in response to cell migration may be required (Worley, Shieh, & Wan, 2015). We found that on glass substrate, $|\Delta\theta|$ was generally reduced not only between direct neighbors but also across a wider range of cell–cell distances. We speculate that the properties of glass substrate, such as rigidity, may upregulate the formation of cadherin-mediated cell–cell contacts, subsequently enhancing intercellular alignment as well as the formation of chiral orientation. Further studies are needed to fully investigate this possibility.

In summary, we here propose a novel framework of image segmentation for the investigation of cell chirality. This automated method allows for the objective and quantitative analysis of cell orientation, enabling the accurate acquisition of alignment angle between closely neighboring cells. Based on the enriched information, intercellular alignment was found to be important in enhancing cells' chiral orientation, suggesting a potential mechanism underlying the development of left–right asymmetry in tissue microarchitecture. We anticipate that by providing greater insight, this method will contribute to studies of cell alignment and chiral orientation, which are important for tissue morphogenesis and regeneration.

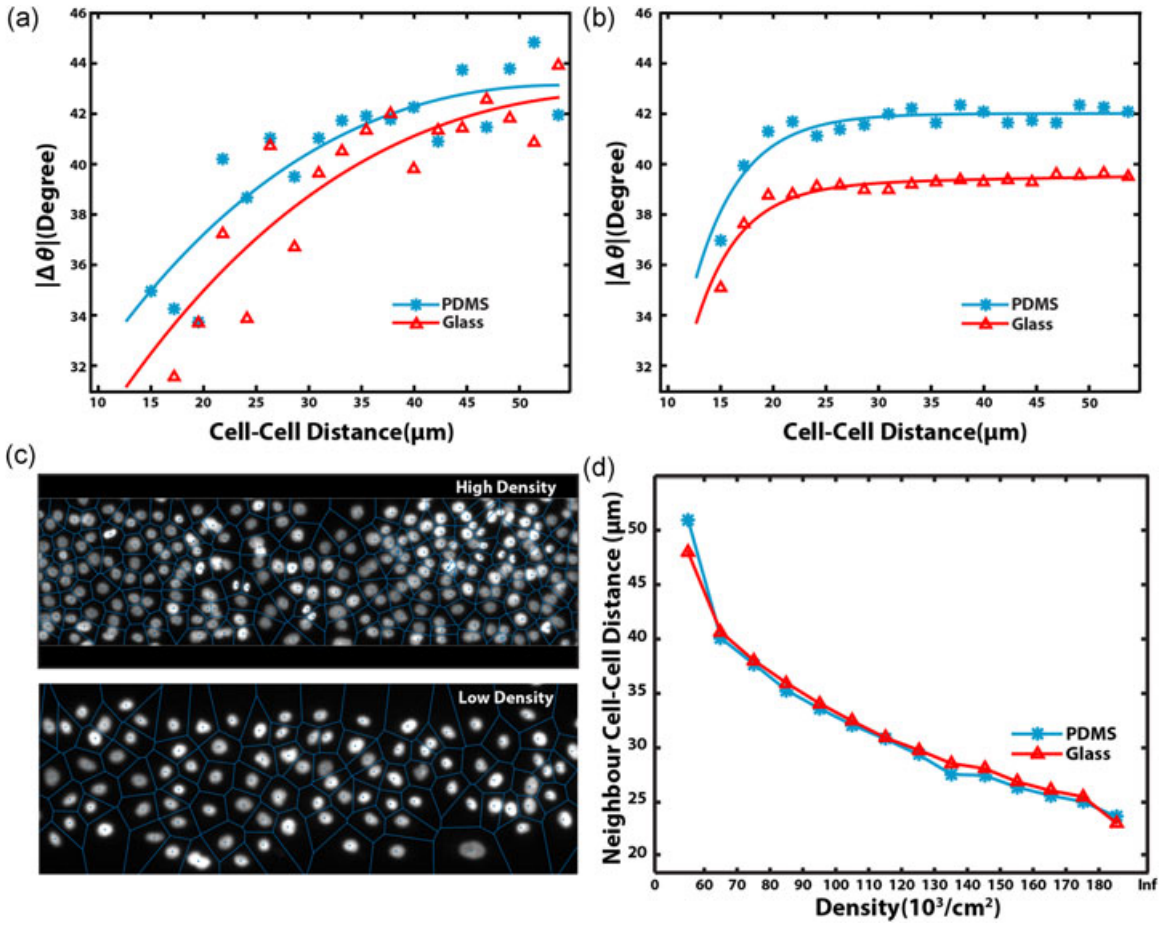

FIGURE 6 Intercellular alignment on substrates with different cell densities. (a,b) For cultures of low cell density (a) and high cell density (b), the averaged, absolute value of acute angle difference $|\Delta\theta|$ among cells and neighboring cells with cell–cell distance <55 μm (120 pixels). (c) Voronoi diagram for images with low and high cell densities. (d) The averaged cell–cell distance between two direct neighbors plotted against cell density [Color figure can be viewed at wileyonlinelibrary.com]

ACKNOWLEDGEMENTS

We acknowledge supports from the National Natural Science Foundation of China (project no. 61502406), the Croucher Foundation (project no. 9500016), the Early Career Scheme (project no. 21214815) and General Research Fund (project nos. 11277516 and 11217217) of the Hong Kong Research Grant Council, and the Science Technology and Innovation Committee of Shenzhen Municipality (grant no. JCYJ20170307091338607).

ORCID

Ting-Hsuan Chen http://orcid.org/0000-0003-4517-7750
Miu Ling Lam http://orcid.org/0000-0002-5333-7454

REFERENCES

Aurenhammer, F. (1991). Voronoi diagrams—A survey of a fundamental geometric data structure. *Computing Surveys*, *23*(3), 345–405. https://doi.org/10.1145/116873.116880

Beucher, S., & Lantuejoul, C. (1979). Use of watersheds in contour detection. *Proceedings of the International Workshop on Image Processing: Real-time Edge and Motion Detection/Estimation*. Rennes, France.

Chen, T. H., Hsu, J. J., Zhao, X., Guo, C., Wong, M. N., Huang, Y., … Demer, L. L. (2012). Left-right symmetry breaking in tissue morphogenesis via cytoskeletal mechanics. *Circulation Research*, *110*(4), 551–559. https://doi.org/10.1161/CIRCRESAHA.111.255927

Chen, T. H., Zhu, X., Pan, L., Zeng, X., Garfinkel, A., Tintut, Y., … Ho, C. M. (2012). Directing tissue morphogenesis via self-assembly of vascular mesenchymal cells. *Biomaterials*, *33*(35), 9019–9026.

Cheng, J., & Rajapakse, J. C. (2009). Segmentation of clustered nuclei with shape markers and marking function. *IEEE Transactions on Biomedical Engineering*, *56*(3), 741–748. https://doi.org/10.1109/TBME.2008.2008635

Chiu, J. J., Chen, L. J., Chen, C. N., Lee, P. L., & Lee, C. I. (2004). A model for studying the effect of shear stress on interactions between vascular endothelial cells and smooth muscle cells. *Journal of Biomechanics*, *37*(4), 531–539. https://doi.org/10.1016/j.jbiomech.2003.08.012

Edelstein-Keshet, L., & Ermentrout, G. B. (1990). Contact response of cells can mediate morphogenetic pattern formation. *Differentiation*, *45*(3), 147–159. https://doi.org/10.1111/j.1432-0436.1990.tb00468.x

Junkin, M., Leung, S. L., Whitman, S., Gregorio, C. C., & Wong, P. K. (2011). Cellular self-organization by autocatalytic alignment feedback. *Journal of Cell Science*, *124*(24), 4213–4220. https://doi.org/10.1242/jcs.088898

Kim, D. H., Lipke, E. A., Kim, P., Cheong, R., Thompson, S., Delannoy, M., … Levchenko, A. (2010). Nanoscale cues regulate the structure and function of macroscopic cardiac tissue constructs. *Proceedings of the National Academy of Sciences of the United States of America*, *107*(2), 565–570. https://doi.org/10.1073/pnas.0906504107

Litjens, G., Kooi, T., Bejnordi, B. E., Setio, A. A. A., Ciompi, F., Ghafoorian, M., … Sánchez, C. I. (2017). A survey on deep learning in medical image analysis. *Medical Image Analysis*, *42*, 60–88. https://doi.org/10.1016/j.media.2017.07.005

Meyer, F. (1994). Topographic distance and watershed lines. *Signal Processing*, *38*(1), 113–125. https://doi.org/10.1016/0165-1684(94)90060-4

Otsu, N. (1979). A threshold selection method from gray-level histograms. *IEEE Transactions on Systems, Man and Cybernetics*, *9*(1), 62–66. https://doi.org/10.1109/tsmc.1979.4310076

Raymond, M. J., Jr., Ray, P., Kaur, G., Singh, A. V., & Wan, L. Q. (2016). Cellular and nuclear alignment analysis for determining epithelial cell chirality. *Annals of Biomedical Engineering*, *44*(5), 1475–1486. https://doi.org/10.1007/s10439-015-1431-3

Ronneberger, O., Fischer, P., & Brox, T. (2015). U-Net: Convolutional networks for biomedical image segmentation. In N. Navab, J. Hornegger, W. M. Wells, & A. F. Frangi (Eds.), *Lecture Notes in Computer Sciences, Vol. 9351. International Conference on Medical Image Computing and Computer-assisted Intervention* (pp. 234–241). Berlin: Springer. doi: https://doi.org/10.1007/978-3-319-24574-4_28

Streeter, D. D., Jr., Spotnitz, H. M., Patel, D. P., Ross, J., Jr., & Sonnenblick, E. H. (1969). Fiber orientation in the canine left ventricle during diastole and systole. *Circulation Research*, *24*(3), 339–347. https://doi.org/10.1161/01.RES.24.3.339

Vunjak-Novakovic, G., Altman, G., Horan, R., & Kaplan, D. L. (2004). Tissue engineering of ligaments. *Annual Review of Biomedical Engineering*, *6*, 131–156. https://doi.org/10.1146/annurev.bioeng.6.040803.140037

Wan, L. Q., Ronaldson, K., Park, M., Taylor, G., Zhang, Y., Gimble, J. M., & Vunjak-Novakovic, G. (2011). Micropatterned mammalian cells exhibit phenotype-specific left-right asymmetry. *Proceedings of the National Academy of Sciences of the United States of America*, *108*(30), 12295–12300. https://doi.org/10.1073/pnas.1103834108

Wang, L., Li, Y., Chen, B., Liu, S., Li, M., Zheng, L., … Xu, F. (2015). Patterning cellular alignment through stretching hydrogels with programmable strain gradients. *ACS Applied Materials & Interfaces*, *7*(27), 15088–15097. https://doi.org/10.1021/acsami.5b04450

Worley, K. E., Shieh, D., & Wan, L. Q. (2015). Inhibition of cell–cell adhesion impairs directional epithelial migration on micropatterned surfaces. *Integrative Biology*, *7*(5), 580–590. https://doi.org/10.1039/C5IB00073D

Zhu, N. H., Kwong, H. K., Bao, Y., & Chen, T. H. (2017). Chiral orientation of skeletal muscle cells requires rigid substrate. *Micromachines*, *8*(6), 181. https://doi.org/10.3390/mi8060181

SUPPORTING INFORMATION

Additional supporting information may be found online in the Supporting Information section at the end of the article.

How to cite this article: Huang Y, Bao Y, Kwong HK, Chen T-H, Lam ML. Outline-etching image segmentation reveals enhanced cell chirality through intercellular alignment. *Biotechnology and Bioengineering*. 2018;115:2595–2603. https://doi.org/10.1002/bit.26783